Corrosion and scale inhibition of low carbon steel in cooling water system by 2-propargyl-5-o-hydroxyphenyltetrazole

N. Dkhireche, A. Dahami, A. Rochdi, J. Hmimou, R. Touir, M. Ebn Touhami, M. El Bakri, A. El Hallaoui, A. Anouar, Hisasi Takenouti

Corrosion and scale inhibition of low carbon steel in cooling water system by 2-propargyl-5-o-hydroxyphenyltetrazole

N. Dkhireche[1], A. Dahami[1], A. Rochdi[1], J. Hmimou[2], R. Touir[1], M. Ebn Touhami[1,*], M. El Bakri[1], A. El Hallaoui[3], A. Anouar[3], H. Takenouti[4]

1- Laboratoire de Matériaux, d'Electrochimie et d'Environnement, Faculté des Sciences, Université Ibn Tofail, BP 133, Kénitra 14 000, Morocco.

2- Laboratoire de synthèse organique et procédés d'extraction. Faculté des Sciences, Université Ibn Tofail, BP 133 Kénitra 14 000, Morocco.

3- Laboratoire de Chimie Organique, Faculté des Sciences Dhar El Mahraz, Université Sidi Mohamed Ben Abdellah.30000, Fès - Morocco.

4- Laboratoire Interfaces et Systèmes Electrochimiques, Université Paris 6, CNRS – France

Abstract

The 2-propargyl-5-o-hydroxyphenyltetrazole (PHPT) has been tested as corrosion inhibitor for low carbon steel in simulated cooling water. The polarization curves showed that PHPT acts as mixed-type inhibitor. Its inhibition efficiency was found to enhance with increase of the inhibitor concentration and immersion time due to the formation of the inhibitor film on the metal surface as indicated by electrochemical impedance spectroscopy measurements.

To complete the formulation further, a non oxidizing biocide was added. Its presence with PHPT does not affect its inhibitory performance and it can be served as a basic component of the formulation for cooling water system.

Keywords: PHPT; Corrosion inhibition; Biocide; Cooling water;

Corresponding authors: Pr. M. Ebn Touhami, Tel.: +212 6 6158 63 00.

E-mail address: mebntouhami@yahoo.fr

1. Introduction

Circulating cooling water system is widely used in industrial processes and central air conditioning system because of its high water upkeep efficiency and rejection of thermal pollution of receiving water compared to once through cooling water system **[1,2]**. In this system, carbon steel is widely used as structural materials. Nevertheless, circulating cooling water system encounters three major problems such as corrosion, scaling, and microbial growth. Most of the well-known inhibitors are organic compounds containing nitrogen, sulfur, and oxygen atoms. Indeed, compounds with functional groups containing hetero-atoms which can donate lone pair electrons are found to be particularly useful as inhibitors for corrosion of metals **[3, 6].** These compounds are still continuously investigated as inhibitors for corrosion of metals in industry. The selection criteria for various inhibitors include low concentration, stability in recirculation, and cost effectiveness.

Tetrazole derivatives on corrosion inhibition of metals in acids **[7-9]** and neutrals [**10-11**] media have been investigated in considerable detail. For example, El-Sayed et al. **[12-13**] studied the effect of 5-(3-aminophenyl)-tetrazole addition on corrosion of copper and iron in aerated 3 % NaCl media at different pH values, using electrochemical and weight loss measurements coupled to Raman spectroscopy analysis. They have found that these compounds are good inhibitors for both metals and their inhibition efficiencies became greater with concentration and immersion time. They reported also that the iron corrosion inhibition was achieved by adsorption of molecules on the metal surface.

At first, the evaluation of propargyl-hydroxyphenyltetrazole (PHPT) as an inhibitor and cetyltrimethylammonium bromide (CTAB) as a microbial growth inhibitor for low carbon steel in simulated cooling water system was investigated. The influence of some operational parameters on its inhibition efficiency was also evaluated using electrochemical methods including potentiodynamic polarization and electrochemical impedance spectroscopy measurements.

2. Experimental procedures

2.1. Electrochemical cell and materials

The electrolysis cell was a borrosilcate glass (Pyrex®) cylinder closed by cap with five apertures. Three of them were used for the electrode insertions. The working electrode was a low carbon steel previously **[14-16]** and its composition is summarized in Table 1. The investigated area of the surface was 0.8 cm^2. Prior to immersion test, the electrode was

abraded using emery paper up to 1200 grade, cleaned with acetone, washed with distilled water, and dried finally. The rotating electrode (INF-EL-EDI 101) was used for electrochemical measurements. The rotation speed was fixed at 1000 rpm with CTV 101 (Radiometer analytical).

Pt plate as the counter while a saturated calomel electrode (SCE) was used as the reference electrode. All potentials are referred with respect to this electrode. For long exposure experiments, between two measurements, the reference electrode was removed from the test solution to minimize its contamination by chloride ions and the working electrode was set in rotation for one hour before each test.

The simulated cooling water solution was used previously **[14-16]** and its composition is displayed in Table 2. This composition represents the average amount of various ions present in the waters used in Moroccan cooling waters system. According to the literature **[17, 18]**, this solution was corrosive and scaling. The temperature was adjusted at 32±1 °C except for the study on the temperature effect. The electrolyte was in contact with air without any purging of dissolved oxygen.

The 2-propargyl-5-o-hydroxyphenyltetrazole (M = 189 g/mol, Melting point = 77 °C, not soluble in water), was used as a corrosion and a scale inhibitor. For a new synthesis method of this substance **[19]** leading the yield of 81%; was as follows : 10 mmol of 5-o-hydroxyphenyltetrazole and 25 ml of anhydrous acetone were added to 11 mmol of K_2CO_3 and the mixture was stirred for 15 minutes. After this, 10 mmol of propargyl bromide was added and the reaction mixture was stirred at room temperature for 2 h. Then, the solvent was evaporated. The obtained residues were taken up in ethyl acetate and were washed into the water for three times. Finally, the organic layers were combined, dried with Na_2SO_4 and were evaporated. The toxicity of 2-propargyl-5-o-hydroxyphenyltetrazole was not yet evaluated.

The cetyltrimethylammonium bromide ($C_{19}H_{42}BrN$), is a commercial product, courteously purchased from FLUKA Company (Denmark), its purity is 96 % and was used as corrosion and biofilm inhibitor. It was evaluated using the minimal inhibitory concentration (MIC) techniques **[20, 21]**. The chemical structures of these two compounds are presented in Fig. 1.

2.2. Polarization measurements

The working electrode was immersed in test solution under rotation at 1000 rpm during one hour until the steady state corrosion potential (E_{corr}) was reached. The cathodic polarization curve was recorded by polarization from E_{corr} towards more negative direction with a sweep

rate of 1 mV/s. After this scan, the same electrode was remained in solution until the obtaining of the steady state corrosion potential (E_{corr} ± 0.002 V), and then the anodic polarization curve was recorded from E_{corr} to positive direction with the same sweep rate. The obtained polarization curves were corrected for ohmic drop with the electrolyte resistance determined by electrochemical impedance spectroscopy. These measurements were carried out using Potentiostat/Galvanostat/Voltalab PGZ 100 monitored by a personal computer. For each concentration three independent experiments were performed. The mean values and the standard deviations are reported as well.

The overall current density values, i, were considered as the sum of two contributions, anodic and cathodic current i_a and i_c, respectively. For the potential domain not too far from the open circuit, it may be considering that both processes follow the Tafel law [**22**]. Thus, it can be derive :

$$i = i_a + i_b = i_{corr}.\{\exp[b_a.(E - E_{corr})] - \exp[b_c.(E - E_{corr})]\} \quad (1)$$

where i_{corr} is the corrosion current density (A.cm^{-2}), b_a and b_c are respectively the Tafel constant of anodic and cathodic reactions (V^{-1}). These constant are linked to the Tafel slope β (V/dec) in usual logarithmic scale by:

$$\beta = \frac{\ln(10)}{b} = \frac{2.303}{b} \quad (2)$$

The corrosion parameters were then evaluated by means of nonlinear least square method by applying this equation using Origin software. However, for this calculation, the potential range applied was limited to ±0.100V around the E_{corr} else a significant systematic divergence was sometimes observed for both anodic and cathodic branches.

The inhibition efficiency (η) was calculated using the following equation :

$$\eta = \frac{i_{corr}^0 - i_{corr}}{i_{corr}^0} \times 100 \quad (3)$$

where i_{corr}^0 and i_{corr} are the corrosion current density values without and with the inhibitor, respectively.

2.3. EIS measurements

The electrochemical impedance spectroscopy measurements were carried out using a transfer function analyzer (Voltalab PGZ 100, Radiometer Analytical), over the frequency range from

100 kHz to 0.01 Hz with 10 points per decade. The applied amplitude of AC signal was 10 mV_{rms}. All experiments were performed at the open circuit potential. The obtained impedance data were analyzed in term of equivalent electrical circuit using Bouckamp's program **[23].** The inhibition efficiency was evaluated with the relationship:

$$\eta = \frac{R_{ct} - R_{ct}^0}{R_{ct}} \times 100 \qquad (4)$$

where R_{ct}^0 and R_{ct} are the charge transfer resistance values in the absence and in the presence of inhibitor, respectively.

3. Results and discussion

3.1. Polarization curves

Fig. 2 presents polarization obtained with a low carbon steel in cooling water system containing different concentrations of PHPT. It can be remarked that both anodic and cathodic branches do not exhibit well-defined Tafel region. As a guide to the corrosion behavior of low carbon steel (predominantly Fe), these results are analysed with Pourbaix diagram for iron **[24]**. According to this diagram, the anodic reaction is the iron dissolution to form Fe^{2+} ions. The main cathodic process is the reduction of dissolved oxygen **[25]**. In addition, it is noted that the anodic branches are curved. This can be explained by deposition of a non- passivating film on the electrode **[26]**. Alternatively, a higher localized pH at cathodic sites (resulting from generation of HO^- ions) can be result in uniform deposition of hydrated iron oxide on the electrode surface **[27]**.

For the blank solution, the cathodic plateau current density ≈ - 800 µA cm^{-2} (Fig. 2) corresponding to the diffusion limited reduction current of dissolved oxygen on bare metal surface.

Besides, it can be seen that with addition of PHPT, both anodic and cathodic branches shift towards smaller current densities and no limiting current plateau was observed.

To yield quantitative approach, i_{corr}, E_{corr}, b_a and b_c were evaluated from the experimental results using a user defined function of "Non-linear least squares curve fit" (Eq. (1)) of graphic software (Origin, OriginLab). In all cases, the correlation factor R^2 is greater than 0.99 indicating a reliable result. Fig. 3 shows, as for an example, the results of regressions calculation for the cathodic and anodic branches in the presence of PHPT at different concentration. In this calculation, the potential domain is limited to E_{corr} ± 100 mV as

mentioned in our previous work **[28]**. A good agreement between the calculated and the experimental polarization data was obtained as trusted in Fig.3.

Table 3 summarizes various corrosion kinetic parameters thus obtained. E_{corr} and the kinetic parameters calculated by a nonlinear regression calculation from the anodic polarization scans near the open circuit potential are similar to those determined from the cathodic polarization scans, though i_{corr} is slightly higher. It can be noticed that both anodic and cathodic current densities decrease gradually by addition of PHPT and the corrosion potentials (E_{corr}) were shifted towards the direction of more noble values. The PHPT may thus be considered as a mixed inhibitor.

It can be seen from Table 3, inhibition efficiency values increase with the increase of inhibitor concentration. This might be possible proof that PHPT adsorb on the low carbon steel surface preventing it from corrosion. It is worth indicating that with increase of the inhibitor concentration, the E_{corr} values shifted slightly towards more positive values whereas the i_{corr} values decrease significantly. Regarding Tafel slope, it can be noticed that both anodic (b_a) and cathodic kinetics (b_c) remain unchanged with addition of PHPT. These results indicate that the inhibiting action occurred by simple blocking of the available surface areas **[29, 30]**. This behaviour can be attributed as well as the formation of inhibitor file as to the presence of nitrogen and oxygen atoms within functional groups (O–H, C=C, C–H, C–O) and aromatic ring (Fig.1), which meets the general requirements of typical corrosion inhibitor.

However in our previous study **[14]**, it was found that the low carbon steel surface is positively charged at the open circuit potential. Thus, in neutral media, the non-bonded electrons of oxygen are ionized ($-O^-$ form). Due to electrostatic interaction, the ionized molecules' constituents are adsorbed (physisorption) to induce the inhibition effect. The adsorption of PHPT from the aqueous solution can be regarded as a quasi substitution process between the inhibitor in the solution and the chloride, sulfate or water molecule at the metal surface.

3.2. Electrochemical impedance spectroscopy

In order to confirm the results extracted from polarization curve and to acquire more information about corrosion mechanisms, EIS measurements were carried out at corrosion potential. The obtained results after immersion in test solution with and without PHPT under rotation at 1000 rpm for one hour are presented in Fig. 4.

In the absence of PHPT, an inductive loop at low frequency-end was observed, but in its presence this feature is transformed to a capacitive behaviour. The origin of this low frequency contribution remains unclear, and we will omit the further analyses. For the frequency higher than 0.1 Hz, in Nyquist plots the impedance are characterized by a depressed capacitive loop. This loop can be split into two capacitive contributions, although badly separated. Because of this poor separation and in order to analyze the Nyquist plots impedance spectra more quantitatively, an equivalent electric circuit with two time constants was tried to reproduce these results by non linear regression calculation. This circuit for the impedance diagrams presented in Fig. 4 is shown in Fig. 5. Where R_s indicates the electrolyte resistance; R_f is the resistance associated with the corrosion product layer formed with some amount of PHPT as can be deduced from EDX analyses; C_f is that associated with the capacitance of this layer; R_{ct} stands for the charge transfer resistance; C_{ct} is attributed to the double-layer capacitance. We will show the comparison of experimental and the calculated EIS data (Fig.4). It can be readily seen that the agreement between two spectra are satisfactory. The minimizing function is the real and the imaginary component of the impedance divided by the impedance modulus for each frequency in percent. χ obtained is 0.9 to 1 (%) trusting that the equivalent circuit used are correct.

The significant data for the corrosion rate obtained from the equivalent circuit approach are presented in Table 4. It can be noted that the capacitance value for the blank solution (C_{ct} = 1741 μF cm^{-2}) is too high to be attributed solely to the double-layer capacitance for metal / solution interface. This capacitance usually valued between 20 and 60 μF cm^{-2} **[32]**. This increase in C_{ct} likely results from the formation of coarse corrosion products (and scale) on low carbon steel surface during its dissolution, therefore leading to an increase of the expanded surface area **[33, 34]**.

It can be seen also that R_{ct} values became greater with increase of PHPT concentration indicating that PHPT has a protective character. Jointly, the film resistance R_f values increase also with PHPT concentration whereas the C_f values decrease. It is also noted that the electrolyte resistance, R_s, values increase with PHPT concentration indicating its adsorption on metallic surface. The surface film formed in presence of inhibitor is therefore thicker and less permeable. The similar results were observed when we studied the phosphonate derivative effect in simulated cooling water **[15, 35].**

In addition, if the planar condenser model was applied to evaluate the thickness of the surface film with the relative dielectric constant of iron oxide equal to 14.2. it can be found that the

thickness of the surface film equal 3.5 μm in the presence of 5×10^{-3} M of PHTP. This value is certainly underestimated since the hydration of the surface film is neglected here.

3.3. Effect of temperature

Figs. 6 and 7 present the polarization curves for low carbon steel in simulated cooling water without and with 5×10^{-3} M of PHPT after one hour of immersion at corrosion potential and under rotation at 1000 rpm at different temperatures range (305–335 K). This temperature range was selected since in cooling systems the water temperature may reach by 332. It is noted that the curves do not exhibit linear Tafel region neither in anodic nor in cathodic domain.

In the absence of PHPT (Fig. 6), a current plateau was observed and it was ascribed to the diffusion limiting current of the dissolved oxygen reduction. For the anodic branch, it is noted that the curves do not exhibit linear Tafel region. In addition, the corrosion potential E_{corr} shifts toward more negative potential when the temperature increased. This can be explained by the enhancement of the anodic dissolution rate of low carbon steel with the temperature increase.

In the presence of 5×10^{-3} M of PHPT (Fig. 7), the corrosion potential E_{corr} shifts toward more negative potential and the current density i_{corr} decreases. It is important to point out that the anodic Tafel slope changes. In the cathodic branch, no current plateau was observed indicating a change in mechanism of oxygen reduction.

Table 5 summarizes the values of corrosion rate extracted from polarization curves at various temperatures. As above, since no neat linear domain was defined, these data were obtained from $E_{corr} \pm 0.100$ V for both anodic and cathodic current branches. In the absence of inhibitor (Fig. 6), it is also seen that the corrosion rate increases with temperature and the plateau cathodic current density appeared clearly. These remarks indicate a diffusion process is prevails at this temperature range. In the presence of inhibitor (Fig.7), the plateau was disappeared. According to Gomma **[36]**, the kinetic of such corrosion acquires the character of a diffusion process in which at lower temperature the quantity of inhibitor present at the metal surface is greater than that at higher temperature. The results show that the inhibition efficiency decreases with temperature indicating that at higher temperatures a dissolution of low carbon steel predominates on inhibitor adsorption.

The apparent activation energy values, E_a, were calculated from the Arrhenius equation:

$$i_{corr} = K_a \exp\left(-\frac{E_a}{RT}\right) \qquad (5)$$

where K_a is the Arrhenius pre-exponential factor, T the absolute temperature and R is the gas constant.

The Arrhenius plot according to equation (5) is presented in Fig. 8. The obtained plots are straight lines and the E_a value was found equal to 15 kJ mol^{-1} in absence of PHPT. In its presence, the E_a value is higher and equal to 52 kJ mol^{-1}. This change may be explained by the modification of the corrosion mechanism. Thus, in absence of PHPT, the corrosion rate was essentially controlled by the diffusion process of dissolved oxygen whereas in its presence, the activation process prevails the corrosion rate in agreement with a low corrosion current density **[37]**.

3.4. Effect of immersion time

Fig. 9 shows the impedance spectra of low carbon steel in simulated cooling water containing 5×10^{-3} M of PHPT at different immersion times under rotation at 1000 rpm. The parameters evolutions with time are summarized in Table 6. The shape of these diagrams is similar to that presented in Fig. 4 at the same PHPT concentration. The charge transfer resistance R_{ct} changes from about 2435 Ω cm^2 after 1 h to approximately 7116 Ω cm^2 after 24 h of immersion. In addition, it is also noted that the electrolyte resistance, R_s, values increase with immersion time. This increase in R_s and R_{ct} can be explained by the protective effect of the PHPT, which is reinforced with the immersion time.

Simultaneously, the film capacitance C_f decreases with immersion time. This decrease may be caused by the decreasing of dissolution reaction extent. Moreover, C_f can be expressed as: $C_f = \varepsilon\varepsilon_0 \times S/d$ (where ε is the relative dielectric constant, ε_0 is the vacuum permittivity, S is the surface area and d is the thickness of the film) **[38]**. Thus, the decrease in C_f parameter can be caused by either decrease of the local dielectric constant or increase of the film thickness **[35]**. The same effect was obtained by Hüsnü Gerengi et al., when they studied the concentration effect of Mimosa extract on brass-MM55 corrosion in 0.5 M H_2SO_4 [**30**].

3.5. Effect of Cl^- ions on PHPT inhibition : Study in 3% NaCl medium

In order to evaluate the PHPT performance, we choose another more aggressive medium such as 3 % NaCl. The potentiodynamic polarization curves of low carbon steel in 3% NaCl

solution without and with 5×10^{-3} M of PHPT at 1000 rpm are presented in Fig.10. The both anodic and cathodic branches show no well defined Tafel region.

It is generally believed that the anodic reaction of iron in aerated neutral chloride media is the dissolution of metallic iron (Fe^0) to ferrous cations (Fe^{2+}) as follows:

$$Fe \longrightarrow Fe^{2+} + 2e^- \qquad (6)$$

This oxidation process also releases electrons, which are consumed at the cathode through a reduction reaction as follows:

$$O_2 + 2\ H_2O + 4e^- \longrightarrow 4\ HO^- \qquad (7)$$

Thus, in the absence of PHPT, the cathodic current follows the Tafel law for $E > -0.7$ V/SCE and the corrosion current density can be determined readily ($i_{corr} \approx 690$ µA cm^{-2}). For the potential more negative than - 0.7 V/SCE, a current plateau was observed and it is ascribed to the diffusion limiting current of the dissolved oxygen reduction (975 $mAcm^{-2}$). In addition, for the anodic branch, neither current fluctuation nor a portion corresponding to pitting corrosion is observed in this range. At the same time, even at the anodic potential close to E_{corr}, the current increases by several orders of magnitude. Then, the anodic current reaches several tens mA cm^{-2}. This increase possibly caused by the Cl^- ions.

In the presence of 5×10^{-3} M of PHPT, the corrosion potential E_{corr} shifts toward more negative potential and the current density i_{corr} decreases. It is important to point out that for potential more positive than - 0.7 V/SCE, the Tafel slope is independent of the inhibitor addition. In contrast, the cathodic curves in more negative potential domain are different in presence and in absence of PHPT. The diffusion limiting current corresponding to the oxygen reduction is not observed in the presence of PHPT. This may be explained by that PHPT also inhibits the oxygen reduction reaction. The simultaneous decrease of both anodic and cathodic current densities in presence of PHPT shows that it behaves like a mixed inhibitor.

As stated above, the cathodic Tafel constant, b_c, remains essentially constant whereas the anodic Tafel constant, b_a, becomes greater in the presence of PHPT (Table 7). This phenomenon can be explained by desorption of the inhibitor when the potential shifted towards more anodic direction as previously reported by Epelboin et al. **[39]**.

3.6. Effect of CTAB on PHPT inhibition

Generally, cooling water systems were affected by different types of bacteria and other microorganisms. For this reason, the biocides were usually added together with corrosion and

scale inhibitors. Then, it appeared necessary to evaluate the effect biocides addition on the inhibitor performance.

To test the influence of biocide on inhibition efficiency of PHPT, 5.49 $\times 10^{-5}$ M of CTAB was added to 5×10^{-3} M of PHPT (mixture). Fig. 11 presents the impedance spectra of low carbon steel, under rotation disc electrode at 1000 rpm, in simulated cooling water in absence and presence of mixture. The obtained results of regression calculation for these spectra are summarized in Table 8.

First of all, it can be remarked from the plot that CTAB acted a corrosion inhibitor even very low concentration (ca. 50 μM) and its efficiency was about 52 %. This result is in agreement with literature **[17, 32, 37]**. It is also seen that in absence of PHPT, no film capacitance was detected but in its presence, the film capacity values decrease with CTAB addition. This may be due to the fact that the film became more thickness in the presence of mixture. On the other hand, the presence of CTAB does not spoil the inhibitive performance of PHPT. Consequently, this mixture can be serve as a basic component for inhibitive formulation for cooling water system.

3.7. Scanning electron microscopy observations and EDX analysis

Fig. 12 presents the scanning electronic microscopy (SEM) images for low carbon steel surface immersed during 2 days in simulated cooling water without and with 5×10^{-3} M of PHPT. The surface micrograph of the inhibitor-free solution (Fig. 12a) shows heterogeneous layer of corrosion and scale products. An EDX analysis (Fig. 13a) identified characteristic corrosion products elements (Fe, O and C) as well as the presence of calcium and magnesium on this layer (scale products). It is also seen that Fe peak is lower indicating a formation of thick layer of corrosion and scale products.

On the contrary, the surface micrograph in the presence of 5×10^{-3} M of PHPT (Fig. 12b) shows a large area free from corrosion and scale products. PHPT is actually an efficient corrosion and scale inhibitor. An EDX analysis (Fig. 13b) showed that Fe peak intensity increased compared to the inhibitor-free solution indicating the absence of thick corrosion and scale layer. It is also noted a marked decrease of Ca peak, and revealed the presence of C, O and N atoms indicating that the presence a thin surface layer formed of PHPT.

4. Conclusion

The corrosion and scale inhibition of low carbon steel in cooling water system by PHPT were investigated. The polarization curves indicated that the PHPT acts as a mixed-inhibitor. Both Tafel polarization and electrochemical impedance techniques revealed that the higher the concentration of the PHPT added, the greater was the inhibition efficiency. The inhibition efficiency has also low temperature dependence and increases with immersion time. In addition, the EIS showed that PHPT forms a protective layer on metallic surface explaining by a low C_f values. Thus, the surface film containing PHPT is sufficiently thick to indicate the presence of the organic compound but too thin to be observable by SEM in agreement with the thickness of corrosion product layer evaluated from C_f value. Finally, the biocide addition does not affect the inhibition efficiency of PHPT what allows its utility for cooling water system.

5. References

1. J. K. Kim and R. Smith, Chem. Engin. Sci., 56 (2001) 3641-3658.
2. H. Zeng, J. Lin, C. Ye, L. Tong, X. Chen, F. Yu, J. Electrom. Anal. Appl., 1 (2009) 6-10
3. S. Deng, X. Li, H. Fu, Corros. Sci., 53 (2011) 822-828
4. M. Cenoui, N. Dkhireche, O. Kassou, M. Ebn Touhami, R. Touir, A. Dermaj, N. Hajjaji, J. Mater. Environ. Sci., 1 (2) (2010) 84-95.
5. B. Labriti, N. Dkhireche, R. Touir, M. Ebn Touhami, M. Sfaira, A. El Hallaoui, B. Hammouti, A. Alami, Arab. J. Sci. Eng., 37 (2012) 1293–1303
6. P.K. Gogoi, B. Barhai, Inter. J. Chem., 2 (2010) 138-143
7. El-Sayed M. Sherif, R.M. Erasmus , J.D. Comins , Corros. Sci., 50 (2008) 3439-3445.
8. K.F. Khaled, M.M. Al-Qahtani, Mater. Chem. Phys., 113 (2009) 150-158.
9. S. Deng, X. Li, H. Fu, Corros. Sci., 52 (2010) 3840-3846
10. F. Zucchi, G. Trabanelli, M. Fonsati, Corros. Sci. 38 (1996) 2019-2029.
11. Z. Khiati, A.A. Othman, M. Sanchez-Moreno, M.C. Bernard, S. Joiret, E.M.M. Sutter, V. Vivier, Corros. Sci., 53 (2011) 3092-3099.
12. El-Sayed M. Sherif, R.M. Erasmus , J.D. Comins , Appl. Electrochem., 39(2009) 83-91.
13. El-Sayed M. Sherif, Mater. Chem. Phys., 129 (2011) 961-967.
14. R. Touir, M. Cenoui, M. El Bakri, M. Ebn Touhami, Corros. Sci., 50 (2008) 1530–1537.
15. R. Touir, N. Dkhireche, M. Ebn Touhami, M. Lakhrissi, B. Lakhrissi, M. Sfaira, Desalination, 249 (2009) 922–928.

16. N. Dkhireche, R. Abdelhadi, M. Ebn Touhami, H. Oudda, R. Touir, M. Elbakri, M. Sfaira, B. Hammouti, O. Senhaji, R. Taouil, Int. J. Electrochem. Sci., 7 (2012) 5314 - 5330.
17. S. Ramesh, S. Rajeswari, Electrochim. Acta, 49 (2004) 811-820.
18. M. Saremi, C. Dehghanian, M. Mohammadi Sabet, Corr. Sci., 48 (2006) 1404–1412.
19. Y. Aouine, H. Faraj, A. Alami, A. El Hallaoui, A. Elachqar, S. El Hajji, A. Kerbal, B. Labriti, J. Martinez, V. Rolland, J.Mar. Chim. Heterocycl., 7 (2008)44-49.
20. D. J. Choi, S. J. You, J. G. Kim, Mater. Sci. Engin. A, 335(2002) 228–235.
21. G. Lancini, F. Parenti, Determination of the Minimal Inhibitory Concentration in Liquid, Springer, New York, (1988) p.14
22. M. Stern, A.L. Geary, J. Electrochem. Soc. 104 (1957) 56-63
23. A. Bouckamp, Users Manual Equivalent Circuit, Ver. 4.51, 1993.
24. M. Pourbaix, Atlas of Electrochemical Equilibria in Aqueous Solutions, NACE, Houston, (1974).
25. H. J. Flitt, D. P. Schweinsberg, Corros. Sci., 47 (2005) 3034–3052
26. D.A. Jones, Principles and Prevention of Corrosion, Macmillan, New York, (1992) p. 96
27. A. Harris, A. Marshall, Corros. Prev. Contr. (August 1980) 17.
28. A. Majjane, D. Rair, A. Chahine, M. Et-tabirou, M. Ebn Touhami, R. Touir, Corros. Sci., 60 (2012) 98–103.
29. A. Ostovari, S.M. Hoseinieh, M. Peikari, S.R. Shadizadeh, S.J. Hashemi, Corros. Sci., 51 (2009) 1935
30. Hüsnü Gerengi, Katarzyna Schaefer, H.Ibrahim Sahin, J. of Industrial and Engineering Chemistry 18 (2012) 2204–2210.
31. J. Creus, H. Idrissi, H. Mazille, F. Sanchette, P. Jacquot, Thin Solid Films, 346 (1999) 150-154
32. M. Duprat, M.C. Lafont, F. Moran, F. Dabosi, Electrochim. Acta, 30 (1985) 353-365
33. B. Assouli, Z.A. Ait chikh, H. Idrissi, A. Srhiri, Polymer, 42(2001)2449-2454.
34. R. Touir, N. Dkhireche, M. Ebn Touhami, M. Sfaira, O. Senhaji, J.J. Robin, B. Boutevin, M. Cherkaoui, Mater. Chem. Phys., 122 (2010) 1–9.
35. Gamal K. Gomma, Mater. Chem. Phys. 56 (1998) 27-34.
36. M. Bouklah, B. Hammouti, M. Lagrenée, F. Bentiss, Corros. Sci.,48 (2006) 2831–2842.
37. P. Gimenez, D. Petit, M. Badia, Mater. Sci. Forum, 8 (1986) p. 315.
38. I. Epelboin, Ph. Morel, H. Takenouti, J. Electrochem. Soc. 118 (1971) 1282-1987.

39. R. Touir, N. Dkhireche, M. Ebn Touhami, M. El Bakri, A. H. Rochdi, R. Allah Belakhmima, J. of Saudi Chem. Soc., (2011), DOI:10.1016/j.jscs.2011.10.020.

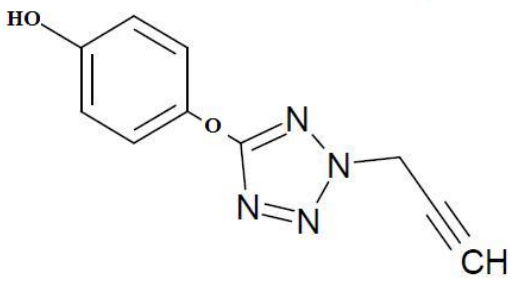

(a)

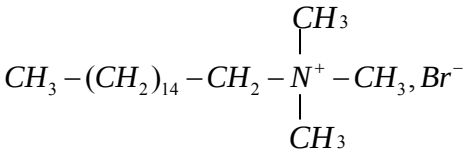

(b)

Fig. 1: Chemical structure of the inhibitors: (a) 2-propargyl-5-o-hydroxyphenyltetrazole (b) cetyltrimethylammonium bromide (CTAB).

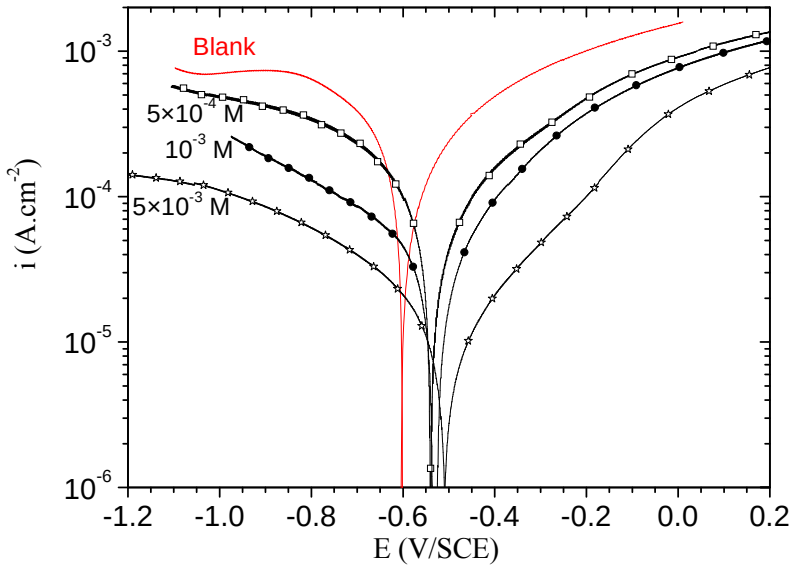

Fig .2: Polarization curves of low carbon steel in cooling water system in the presence of different concentrations of PHPT (T = 305 K; Ω = 1000 rpm).

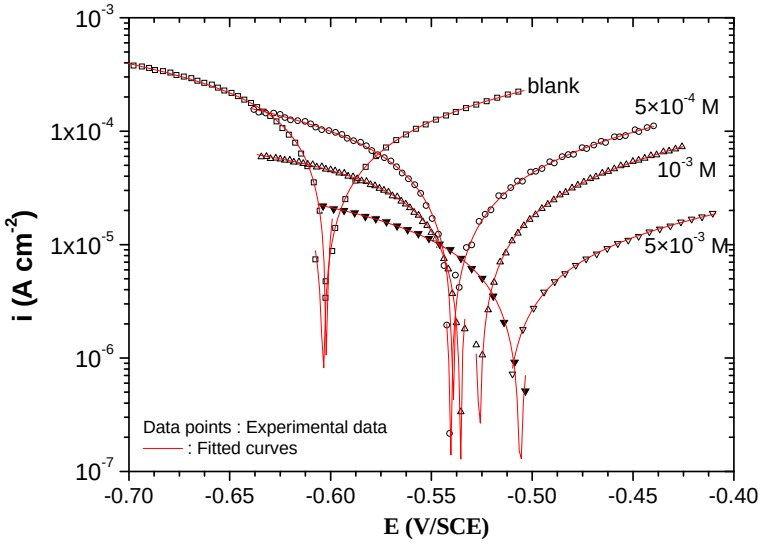

Fig. 3 : Comparison of experimental and fitting data using a non-linear fitting with Stern-Geary equation.

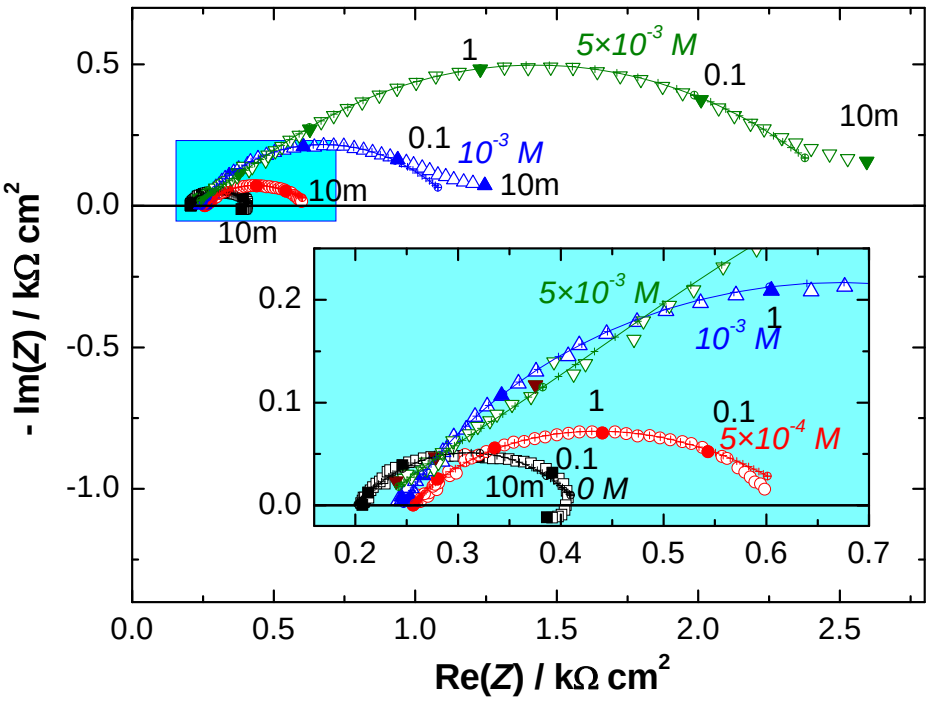

Fig. 4: Comparison of experimental (Symbols) and calculated (+++) EIS according to the electrical equivalent circuit presented in Fig 5 for low carbon steel in simulated cooling water containing different concentrations of PHPT at corrosion potential (T = 305 K; Ω = 1000 rpm). The insert indicates the high frequency domain in enlarged scale.

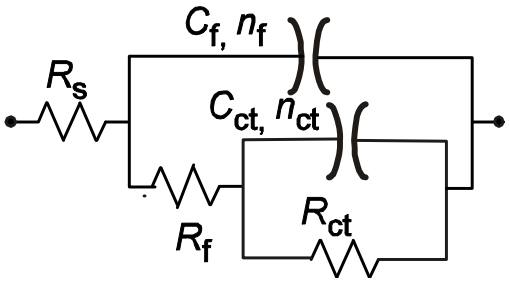

Fig. 5: Electrical equivalent circuit proposed to simulate the impedance diagrams

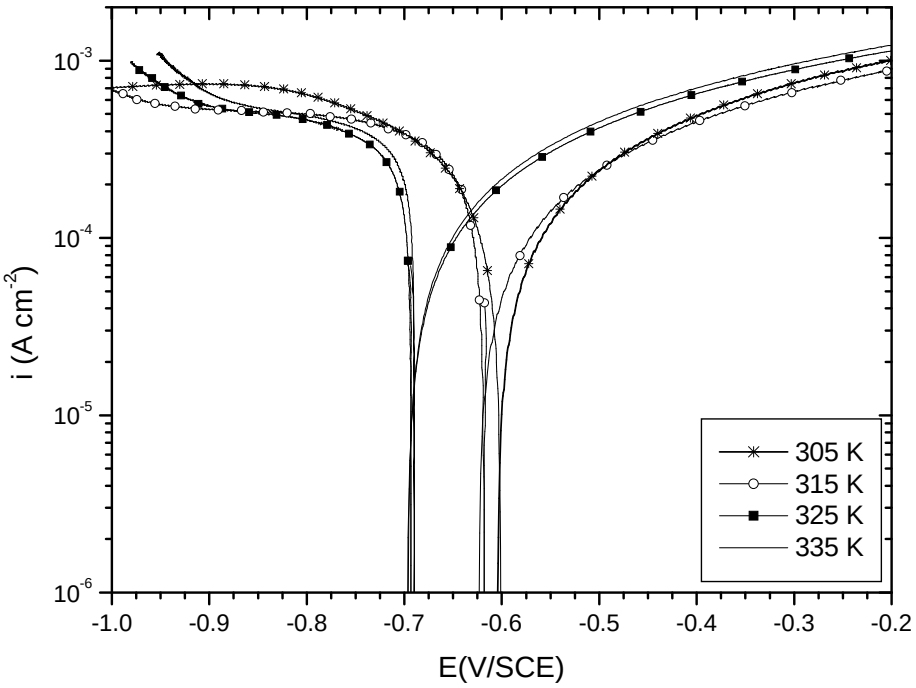

Fig.6 : Temperature effect on the polarization curves of low carbon steel in simulated cooling water without PHPT (Ω = 1000 rpm).

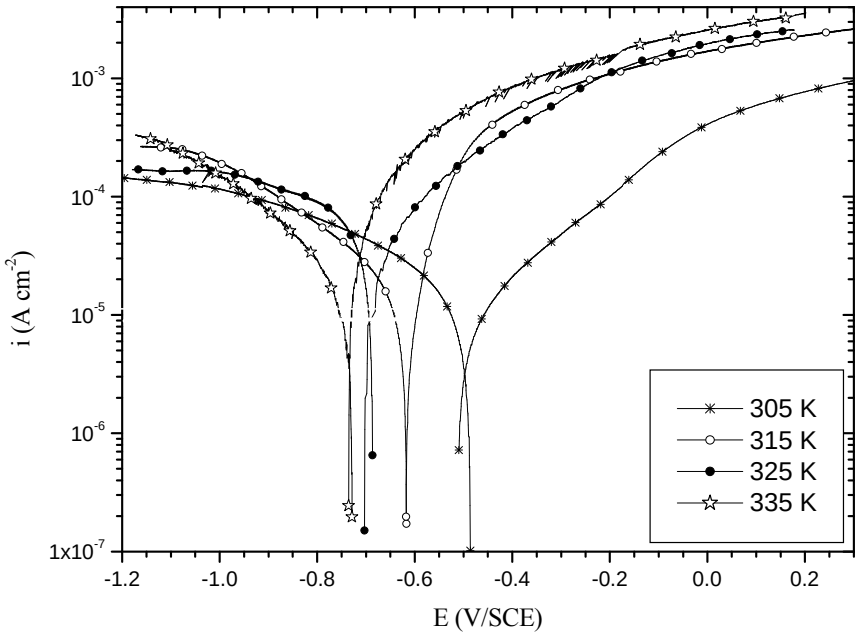

Fig.7 : Temperature effect on the polarization curves of low carbon steel in simulated cooling water with 5×10^{-3} M of PHPT (Ω = 1000 rpm).

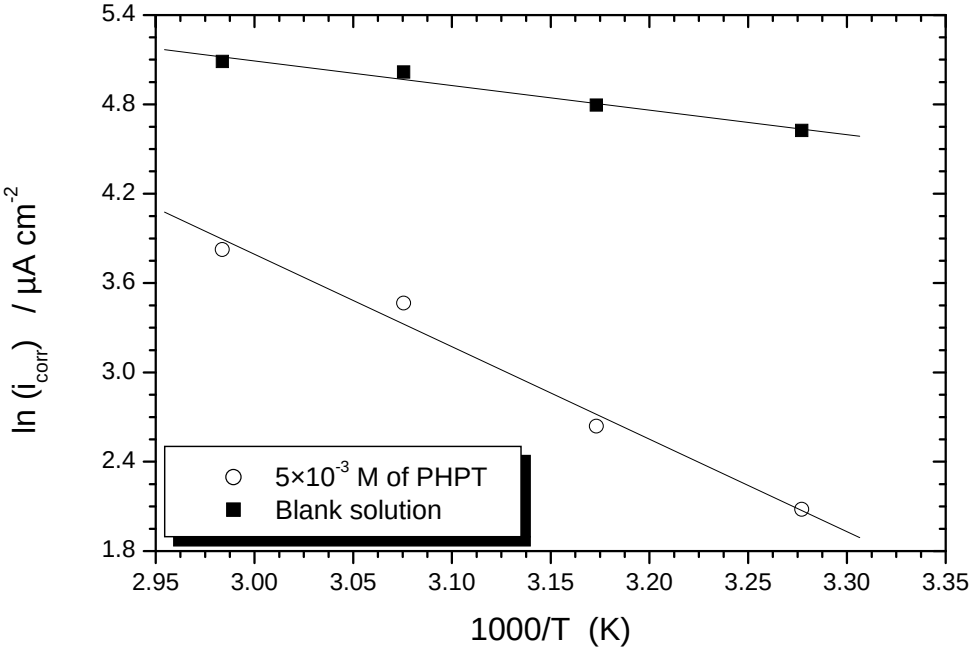

Fig. 8: Arrhenius plot of i_{corr} with and without 5×10^{-3} M of PHPT.

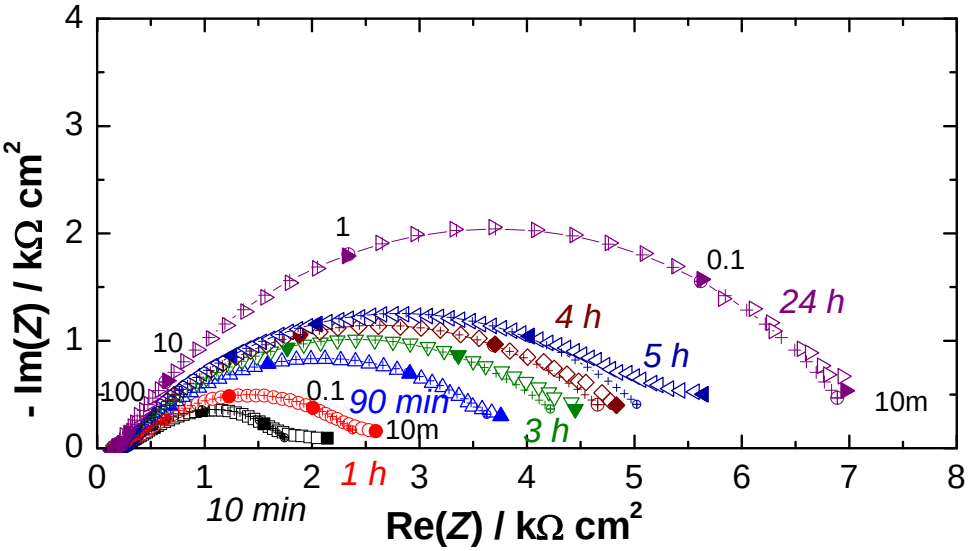

Fig. 9: Comparison of experimental (Symbols) and calculated (+++) EIS according to the electrical equivalent circuit presented in Fig 5 for low carbon steel obtained after different immersion time in simulated cooling water with 5×10^{-3} M of PHPT (T = 305 K; Ω = 1000 rpm).

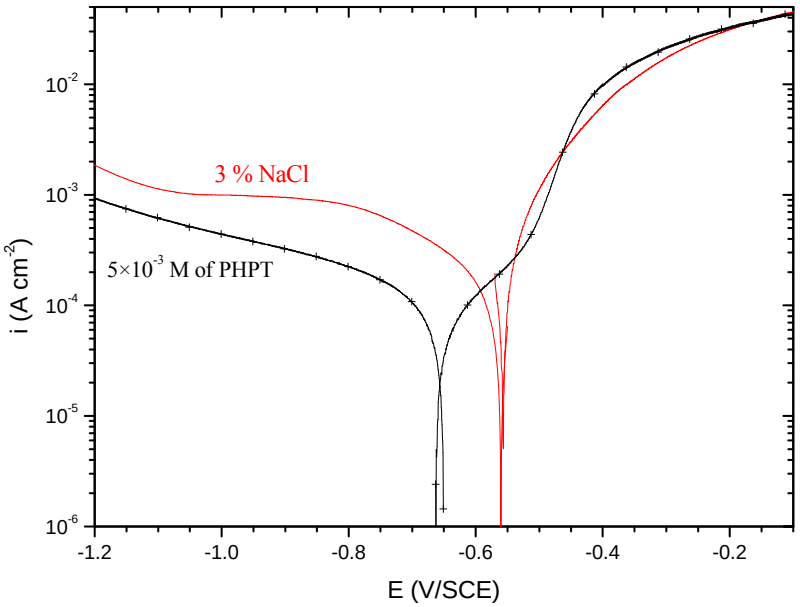

Fig .10: Polarization curves of low carbon steel electrode in 3 % NaCl in absence and in presence of 5×10^{-3} M of PHPT (T = 305 K; Ω = 1000 rpm).

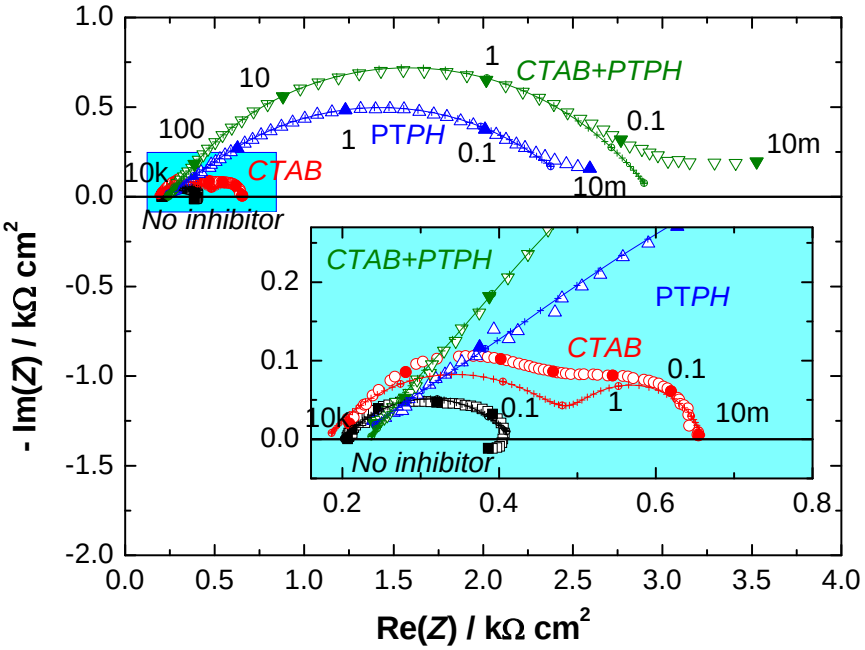

Fig. 11: Comparison of experimental (Symbols) and calculated (+++) EIS according to the electrical equivalent circuit presented in Fig 5 for low carbon steel in simulated cooling water containing 5×10^{-3} M of PHPT with and without 5.49 $\times10^{-5}$ M of CTAB at E_{corr} (T = 305 K; Ω = 1000 rpm). The insert indicates the high frequency domain in enlarged scale.

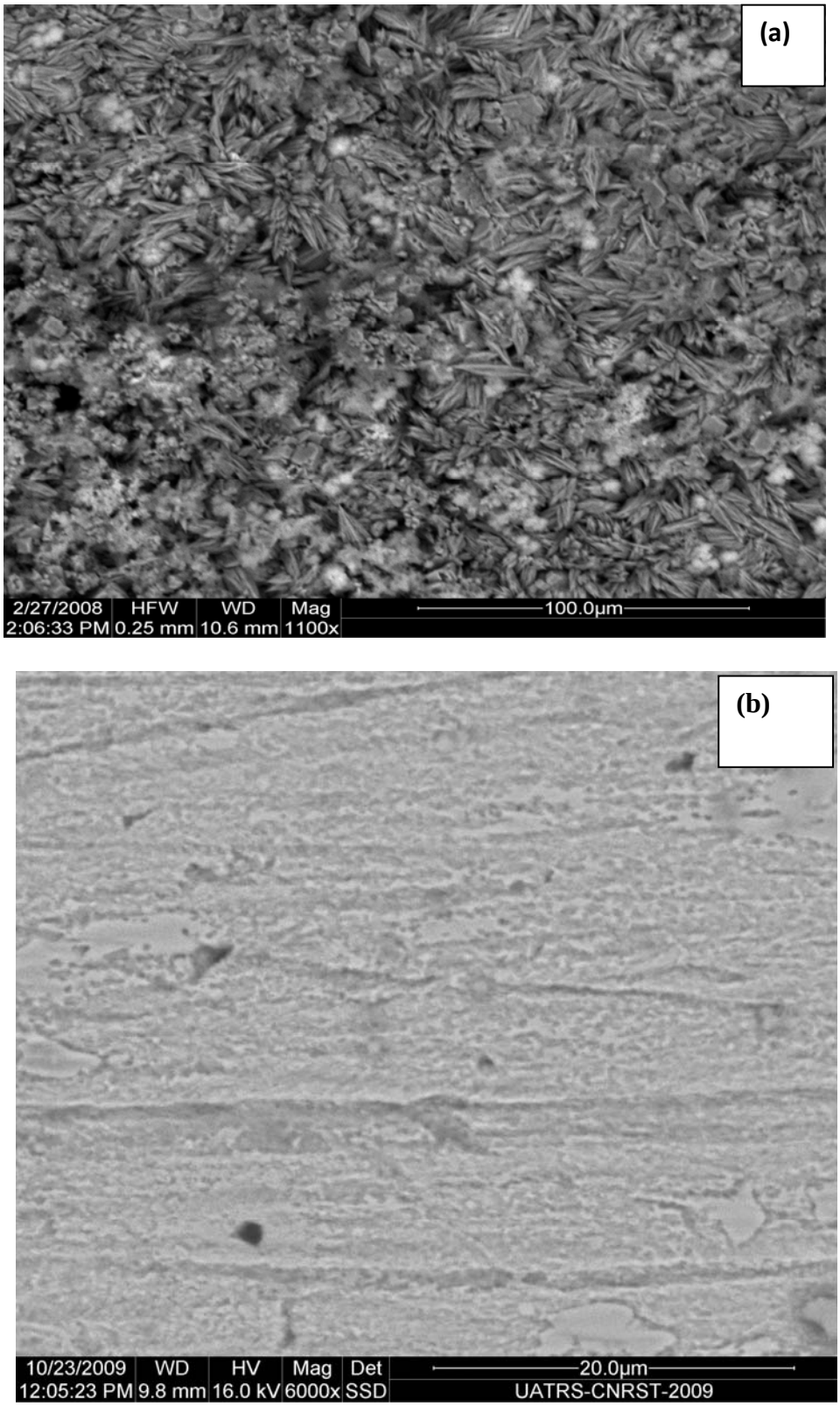

Fig. 12: SEM micrographs of low carbon steel after 2 days of immersion in simulated cooling water: (a) without inhibitor and (b) with 5×10^{-3} M of PHPT.

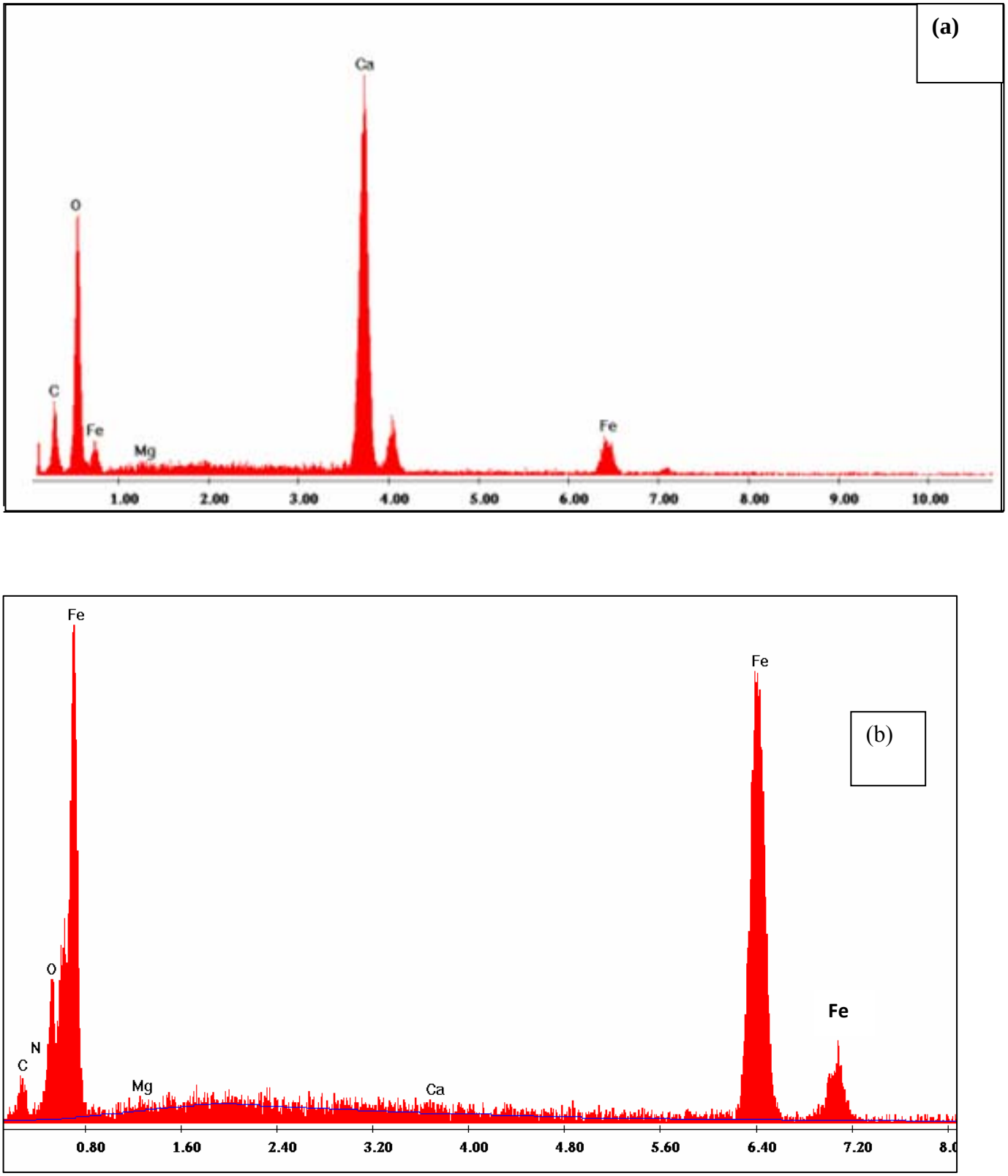

Fig. 13 : EDX analysis of low carbon steel after 2 days of immersion in simulated cooling water: (a) without inhibitor and (b) with 5×10^{-3} M of PHPT.

C	Si	Mn	Cr	Mo	Ni	Al	Cu	Co	V	W	Fe
0.11	0.24	0.47	0.12	0.02	0.1	0.03	0.14	<0.0012	<0.003	0.06	Balance

Table 1. Chemical composition of low carbon steel in wt-%

Salts	$MgCl_2$, $6H_2O$	$CaCl_2$,$2H_2O$	$Ca(NO_3)_2$,$6H_2O$	$MgSO_4$,$7H_2O$	$NaHCO_3$
Concentration (mM)	2.85	3.64	0.566	1.56	3.77
Conductivity ($\mu S\ cm^{-1}$) at 299 K	1678				

Table 2. Composition of simulated cooling water.

Conc. (M)	E_{corr} (mV/SCE)	i_{corr} ($\mu A\ cm^{-2}$)	b_a (1/V)	b_c (1/V)	η %
0	-602	102	5	-4.8	-
5×10^{-4}	-540	47	5.03	-5.02	54
10^{-3}	-534	25	6.26	-4.57	75
5×10^{-3}	-500	8	5.12	-4.41	92

Table 3. Data obtained from polarization curves for low carbon steel in cooling water system containing different concentrations of PHPT (T = 305 K; Ω = 1000 rpm).

Conc. (M)	R_s ($\Omega\ cm^2$)	R_f ($\Omega\ cm^2$)	C_f ($\mu F\ cm^{-2}$)	R_{ct} ($\Omega\ cm^2$)	C_{ct} ($\mu F\ cm^{-2}$)	η %
0	122	-	-	153	1741	-
5×10^{-4}	257	112	2.13	456	531	66
10^{-3}	235	127	1.56	1260	316	88
5×10^{-3}	222	160	0.315	2435	130	94

Table 4. Impedance parameters for low carbon steel in simulated cooling water containing different concentrations of PHPT (T = 305 K; Ω = 1000 rpm).

	T (K)	E_{corr} (mV/SCE)	i_{corr} ($\mu A\ cm^{-2}$)	b_a (1/V)	η %
Blank solution	305	-605	102	5	-
	315	-621	121	2.65	-
	325	-695	151	1.58	-
	335	-698	162	1.37	-
5×10^{-3} M of PHPT	305	-500	8	5.12	92
	315	-622	14	2.65	89
	325	-701	32	2.93	80
	335	-741	46	4.96	72

Table 5. Electrochemical parameters for low carbon steel in simulated cooling water with and without 5×10^{-3} M of PHPT at different temperatures (Ω = 1000 rpm).

Immersion time (h)	R_s ($\Omega\ cm^2$)	R_f ($\Omega\ cm^2$)	C_f ($\mu F\ cm^{-2}$)	R_{ct} ($\Omega\ cm^2$)	C_{ct} ($\mu F\ cm^{-2}$)	η %
1/2	175	121	0.413	1817	175	92
1	222	160	0.315	2435	130	94
3/2	159	118	0.211	3771	105	96
3	153	107	0.118	4594	104	97
4	132	135	0.105	5236	89	97
5	152	210	0.101	5636	75	97
24	139	110	0.025	7116	55	98

Table 6. Impedance parameters of low carbon steel in simulated cooling water with and without 5×10^{-3} M of PHPT at different immersion time (T = 305 K; Ω = 1000 rpm).

	E_{corr} (mV/SCE)	i_{corr} ($\mu A\ cm^{-2}$)	b_a (1/V)	b_c (1/V)	η %
3 % NaCl	-550	690	18	-3.23	-
5×10^{-3} M of PHPT	-663	90	21.8	-3.28	86

Table 7. Electrochemical parameters of low carbon steel in 3 % NaCl with and without 5×10^{-3} M of PHPT (T = 305 K; Ω = 1000 rpm).

	R_s ($\Omega\ cm^2$)	R_f ($\Omega\ cm^2$)	C_f ($\mu F\ cm^{-2}$)	R_{ct} ($\Omega\ cm^2$)	C_{ct} ($\mu F\ cm^{-2}$)	η %
Blank solution	122	-	-	153	1741	-
5.49×10^{-5} M of CTAB	114	-	-	319	238	52
5×10^{-3} M of PHPT	222	160	0.315	2435	130	94
Mixture	215	124	0.081	2900	22	95

Table 8. Electrochemical impedance parameters of low carbon steel in simulated cooling water containing 5×10^{-3} M of PHPT with and without 5.49×10^{-5} M of CTAB (T = 305 K; Ω = 1000 rpm)